JOURNAL OF CATALYSIS 97, 357–365 (1986)

Boron Effects in a Zeolite-Based Hydrotreating Catalyst

MARIO L. OCCELLI[1] AND THOMAS P. DEBIES

Gulf Research & Development Company, P.O. Drawer 2038, Pittsburgh, Pennsylvania 15230

Received December 4, 1984; revised September 3, 1985

A hydrotreating catalyst has been prepared by incorporating HY zeolite (50 wt%) into an Al_2O_3 matrix by a forming method involving peptizing agents, mix-mulling, and a high-temperature calcination step prior to metals loading with 14% Mo and 4% Ni. Electron microprobe measurements indicate that boron (H_3BO_3) addition generates a catalyst with radial concentration gradients; its exterior is metal-rich in molybdenum and nickel. In contrast, if $Al(NO_3)_3$ is used as a peptizing agent, metals (Ni and Mo) are preferentially found in the catalyst interior. X-Ray photoelectron spectroscopy (XPS) indicates that nickel is present as a pseudo-spinel, while molybdenum is present predominantly as a supported oxide. Macroporosity as well as segregation of metals on the surface (induced by H_3BO_3 addition) is believed responsible for the boron-containing catalyst's improved hydrodenitrogenation activity in upgrading vacuum gas oil at mild hydrotreating conditions.

INTRODUCTION

Due to declining petroleum production there is increased interest in generating synthetic fuels and chemical feedstocks from coal liquids and shale oil and to the study of new hydrotreating catalysts and processes to upgrade these nitrogen-contaminated oils (*1*). During hydrodesulfurization (HDS), sulfur removal occurs directly without hydrogenation of the associated aromatic ring (*2*). In contrast, hydrodenitrogenation (HDN) of nitrogen-containing compounds occurs via a complex sequence of reactions involving aromatic ring hydrogenation followed by carbon–nitrogen bond scission (*3–7*). Therefore, it is not surprising that HDN catalysts are generally dual-functional catalysts where hydrogenation reactions occur on impregnated metal centers like Ni–Mo, Co–Mo, or Ni–W combinations (*8, 9*), while hydrogenolysis reactions involve interactions with the support and its acid centers. The acidity function can be provided either by a zeolite, alumina, or by amorphous aluminosilicates (*10, 11*). An appropriate balance between hydrogenation and C–N bond-breaking functions is necessary to provide a catalyst with the appropriate sites for the desired HDN and HDS activity.

Boron's catalytic effects in reducing NO_x impurities from gases is well documented in the patent literature. Aluminum borate is suggested as the active component in various boron-containing catalysts (*12*). Boron–alumina-based hydrocracking (*13*) and hydrorefining (*14–16*) catalysts are examples of industrial applications of boron-containing materials. Recently, Japanese workers used the same type of zeolite-free catalysts to hydrodenitrogenate Arabian light oils (*17–20*). HDN and HDS catalysts prepared by impregnating an alumina support with H_3PO_4 and HBF_4 are described by Pollard and Veorhies (*21*). Pine reported the preparation of zeolite-containing HDN and HDS catalyst by hydrolyzing a mixture of boron-alkoxide and aluminum-alkoxide (*22, 23*).

The literature contains conflicting data on pore size and surface area effects on hydro-treating catalysts' activity (*1*). Livingston (*24*) showed that support properties can have a significant effect on catalyst performance. Other workers (*25*) have reported instead that in the range of 33 to 232 Å, pore size has a negligible effect on the hydro-

[1] To whom all correspondence should be addressed. Present address: 376 S. Valencia Av., UNOCAL, Brea, Ca., 92621.

0021-9517/86 $3.00

denitrogenation of Middle East gas oils, of raw anthracene oil, and for hydrogenation over coal liquefaction catalysts (*25–27*). During hydrodenitrogenation of raw anthracene oil, changes in pore size distribution did not affect nitrogen removal, while a reduction in surface area resulted in a reduction of HDN activity (*1*). Diffusion resistances may cause hydrodesulfurization activity to decrease with catalyst pore size. Hydrodenitrogenation, being slower than hydrodesulfurization, may not be affected by diffusional limitations and thus, within reasonable range variations, catalyst activity is independent of pore size and is more likely to be proportional to the available (active) surface area and metals centers.

EXPERIMENTAL

Catalyst Preparation

Catalysts were prepared by mix-mulling a 50–50% zeolite (Davison ultrastable HY), Catapal alumina mixture with a 1% $Al(NO_3)_3$ or with a 1% H_3BO_3 solution, and then forming the cake into 0.16-cm extrudates with a 2.54-cm bench-scale Bonnot extruder. The matrix was dried and then heat-shocked at 760°C/2 h prior to metal loading with phosphomolybdic acid ($H_3[PMo_{12}O_{40}] \cdot xH_2O$). The Mo-loaded (14 wt% Mo) extrudates were then dried, calcined in air at 480°C/2 h, and impregnated with 4% Ni from $Ni(NO_3)_2$ in a nonaqueous (methanol) solvent. After one final calcination step at 600°C/4 h under nitrogen, the catalysts were submitted for testing. Metals were loaded by the incipient wetness method.

Catalyst Characterization

Surface properties. A DIGISORB 2600 from Micromeritics Instrument Corporation measured N_2 sorption, BET surface area, and pore size distributions. Mercury penetration porosimetry measurements were performed using a Quantachrome porosimeter.

XPS measurements. Spectra were measured with a Physical Electronics Model 550 XPS/SAM/SIMS unit operating at a base pressure of 8×10^{-9} Torr. Samples were irradiated with Mg$K\alpha$ X rays at a power of 300 W. All spectra were calibrated relative to the Al 2*p* line at 74.5 eV. This assumes that the majority of the aluminum signal originates from alumina. Data were collected, processed, and stored by the system's PDP-11/04 computer which is equipped with dual floppy disks. Software enabled treatment of the data including background and X-ray satellite subtraction, smoothing, and semiquantitative analysis. The semiquantitative analysis is based on empirical sensitivity factors employed to correct measured peak areas to yield concentrations in units of atomic percent. The two samples studied were examined either as extrudate samples on tape or as ground extrudates mounted on double-back tape (*28*). The ground samples were prepared to determine the existence of concentration gradient across the catalyst.

Electron microprobe measurements. Compositional information was obtained from microprobe analysis of five pellets from each sample; five successive identical results were taken as evidence of reproducibility and that the material was representative of the catalyst under study. The samples are prepared by cementing the extrudates in hollows drilled into a brass plug and by subsequently polishing the extrudates to a flat smooth finish. The pellets were either gold- or carbon-coated to prevent charging during the experiment. Radial distribution of elements across the extrudate diameter was determined (to an accuracy of 1 μm) with the wavelength dispersive spectrometer attached to the JEOL JSMU-35C Scanning Electron Microscope (SEM).

Reduction measurements. To help identify nickel species, catalysts were reduced in flowing hydrogen at 400°C for 1 h. Hydrogen was purified with an in-line Oxisorb cartridge; flow rate was 10 cm^3/s. Following reduction, the catalyst was transferred to the spectrometer under a nitrogen blanket in a transfer vessel.

TABLE 1

Chargestock Inspection

Inspection	Agha Jari VGO
Gravity, °API	23.2
Sulfur, wt%	1.75
Nitrogen, total, ppm	1500
Nitrogen, basic, ppm	395
C–H Semimicro, wt%	
Carbon	86.09
Hydrogen	12.01
% Carbon residue, rams	0.26
Nickel, ppm	0.7
Vanadium, ppm	1.0
Aniline point, °C	84.5
Distillation, °C	
5	307
10	342
20	380
30	403
40	423
50	438
60	452
70	467
80	485
90	511
95	532
Endpoint	546

Catalyst Testing

Catalyst activity for HDS and HDN of an Agha Jari VGO (Table 1) was evaluated with a 1.75-cm-i.d. reactor having a 0.48-cm thermowell. Thermocouples were positioned in the well to read temperatures at five bed heights. The reactor was loaded with 75 cm^3 of catalyst sized to 20–30 mesh. Each catalyst was then presulfided at 200°C for 4 h with an 8% H_2S–92% H_2 mixture flowing at 2.0 scf/h. Testing conditions were: 2.0 LHSV, 102 atm, and 356 m^3/m^3 (2000 scf/bbl) of once-through 85% H_2–15% CH_4 hydrogen mixture. After 4 h at temperature, products were collected and analyzed every 2 h until constant sulfur levels were observed.

RESULTS AND DISCUSSION

Catalysts with a crush strength resistance of 2.7 atm, 208 m^2/g N_2 surface area, and average pore radius of ~20 Å were obtained when $Al(NO_3)_3$ was the peptizing agent. Variations of surface properties as a function of calcination and metal loading steps are shown in Table 2. Heat treating at 760°C increases catalyst surface area; high

TABLE 2

Surface Properties of a Composite Catalyst as a Function of Temperature and Metal Loadings

	Matrix		Matrix with 14% Mo + 4% Ni	
	Fresh (260°C)	Calcined (760°C)	Metal loaded (260°C)	Metal loaded (480°C)
N_2 pore volume (cm^3/g)	0.46	0.44	0.26	0.28
N_2 pore radius (Å)	25.9	21.4	23.2	21.2
BET area (m^2/g)	356	412	222	208
Pore volume distribution				
R (Å)	Area (%)			
0–10	60.6	58.8	61.2	77.6
10–15	7.0	10.0	8.8	2.3
12–25	4.3	6.4	4.6	1.2
25–30	3.3	4.8	2.9	2.1
>30	24.8	20.0	22.5	16.8

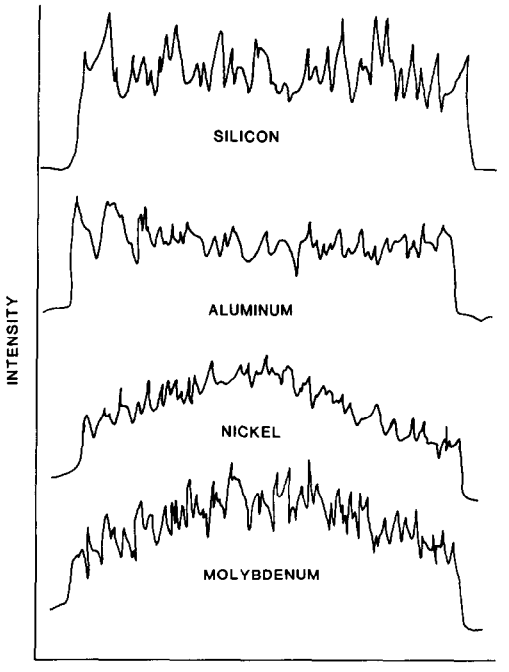

FIG. 1. Microprobe measurements of elemental analysis distribution across the diameter of a zeolite-rich hydrotreating catalyst peptized with 1% Al from $Al(NO_3)_3$.

metals level (14% Mo + 4% Ni) does not cause pore blockage and the N_2 average pore radius stays unchanged at ~21 Å. If $Al(NO_3)_3$ is replaced by H_3BO_3, the boron-promoted composite catalyst is characterized by a N_2 surface area of 169 m^2/g, average pore radius of ~22 Å, and a lower crush strength resistance (~1 atm) due to the presence of macropores. In fact, high pressure (0–60,000 psi) mercury intrusion measurements have shown that approximately 50% of the total Hg pore volume (0.34 cm^3/g) is in pores greater than 1000 Å in diameter; its Hg surface area is 90 m^2/g. In contrast, the stronger $Al(NO_3)_3$ peptized catalyst did not contain measurable macroporosity in this pore size range; 50% of its Hg pore volume (0.22 cm^3/g) was found in pores greater than 110 Å in diameter. This catalyst had a Hg surface area of 86 m^2/g.

Microprobe measurements of Ni and Mo distributions in catalyst pellets are shown in Figs. 1 and 2. These data indicate that the zeolite-rich catalyst peptized with $Al(NO_3)_3$, in addition to having excellent physical properties, has a radial distribution of Ni and Mo which indicate metals segregation to the catalyst interior. With H_3BO_3 as the peptizing agent, greater concentration gradients are established and the catalyst exterior becomes rich in Ni (and to a lesser degree Mo) (see Fig. 2).

XPS survey spectra from 0 to 1000 eV binding energy were measured to determine the catalysts' elemental composition and chemical states (Table 3). Binding energies calibrated relative to the Al 2*p* line of alumina for a number of reference compounds are listed in Table 4. Zeolite contributions to the Al 2*p* signal have no effect on the assumed calibration energy since the zeolite Al 2*p* binding energy is virtually identical to the one exhibited by alumina (see Table 4). Boric acid was originally suspected to be capable of reacting with nickel to form nickel borate, in the same way nickel reacts

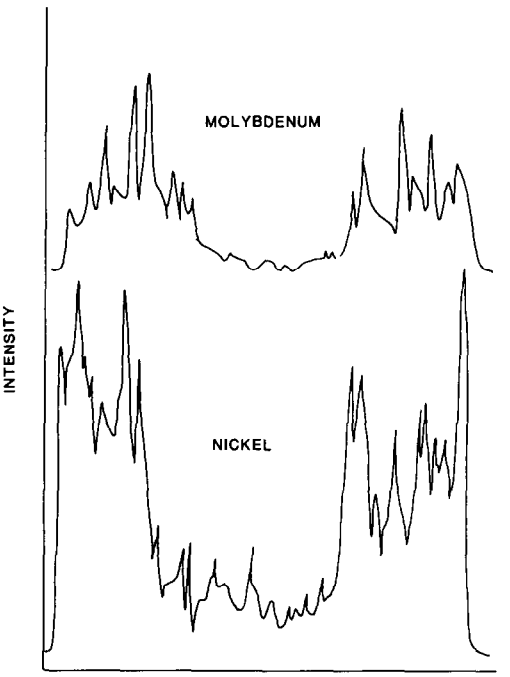

FIG. 2. Microprobe measurements of elemental analysis distribution across the diameter of a zeolite-rich hydrotreating catalyst peptized with 2% B from H_3BO_3.

TABLE 3

Measured Binding Energies

Level	Binding energy (±0.2 eV)		Assignment
	1% Al	2% B	
Al $2p$	74.5	74.5	Alumina
B $1s$	—	192.7	Boric acid
C $1s$	284.0	284.0	Hydrocarbon
	284.4	284.4	contamination
Mo $3d_{5/2}$	232.7	232.5	MoO_3/Al_2O_3
Ni $2p_{3/2}$	856.5	856.6	NiO/Al_2O_3
O $1s$	531.5	531.5	Interacting with support, oxide,
Si $2p$	102.3	102.5	zeolite

with silica to form nickel silicates (*29–31*). The binding energy for nickel borate is not available, but that of sodium borate has been reported as 192.3 eV. The measured binding energy of 192.7 eV agrees with that of boric acid (192.8 eV). In addition, nickel binding energies measured for catalysts with and without boron are identical, suggesting (by inference) that nickel borate is not present, or at least cannot be distinguished.

Prolonged time-averaged scans for nickel resulted in Ni $2p_{3/2}$ spectra resembling those obtained for nickel on alumina. Peak broadening and binding energy elevation indicate strong metal–support interactions and the presence of nickel in two different environments (*32, 33*). Nickel can be found as a pseudo- or surface spinel in which Ni(II) ions are distributed in tetrahedral and octahedral sites left in the interstices of the oxygen anion in a manner similar to a bulk spinel. In the surface spinel, the relative ratios of the tetrahedral and octahedral sites occupied depend strongly on the preparative conditions and the type of support used. In the pseudo-spinel structure, the easily reducible octahedral nickel ions are exposed on the surface while the nonreducible tetrahedral ions are buried beneath the surface (*34, 35*).

Figure 3 shows the Ni $2p_{3/2}$ postreduction spectra measured for the two ground catalysts. Little reduction occurred, suggesting that a small amount of octahedral nickel is present. The Ni $2p_{3/2}$ peak at ~854 eV is assigned to metallic nickel. This result, coupled with the elevated binding energy, satellite intensity, and peak shape is in agreement with the assignment of nickel in both cases to a supported nickel species resembling a pseudo-spinel. Spectra for the sulfided catalysts can be seen in Fig. 4. The peak at 853.9 eV is assigned to Ni_2S_3, the peak at 855.0 eV to NiS or to NiO, and the peak at 857.2 eV to $NiSO_4$ or to NiO interacting with the support. In the B-promoted catalyst Ni is segregated to the exterior where it can be oxidized to $NiSO_4$, when air-exposed (Fig. 4). The Al-peptized catalyst has Ni (and therefore NiS) buried in its interior where oxidation from air exposure is more difficult. Exposure to air could have occurred during the unloading of the hot sulfided catalysts from the pilot plant unit.

TABLE 4

Binding Energies for Reference Compounds

Compound	Level	Binding energy (eV)
Al_2O_3	Al $2p$	74.5[a]
$Na_2B_4O_7$	B $1s$	192.3
$B(OH)_3$	B $1s$	192.8
MoO_3	Mo $3d_{5/2}$	232.5
MoS_2	Mo $3d_{5/2}$	223.9
MoS_2	Mo $3d_{3/2}$	227.1
MoO_3/Al_2O_3	Mo $3d_{5/2}$	232.6
NiO	Ni $2p_{3/2}$	854.5
NiO/Al_2O_3	Ni $2p_{3/2}$	856.7
NiO/SiO_2	Ni $2p_{3/2}$	856.3
NiS	Ni $2p_{3/2}$	854.8
$NiSO_4$	Ni $2p_{3/2}$	857.2
Al_2O_3	O $1s$	531.5
SiO_2	Si $2p$	103.4
Zeolites	Si $2p$	102.4
Zeolites	Al $2p$	74.4

[a] Handbook of X-Ray Photoelectron Spectroscopy," Perkin–Elmer Physical Electronic Division, Eden Prarie, Minn. (1979).

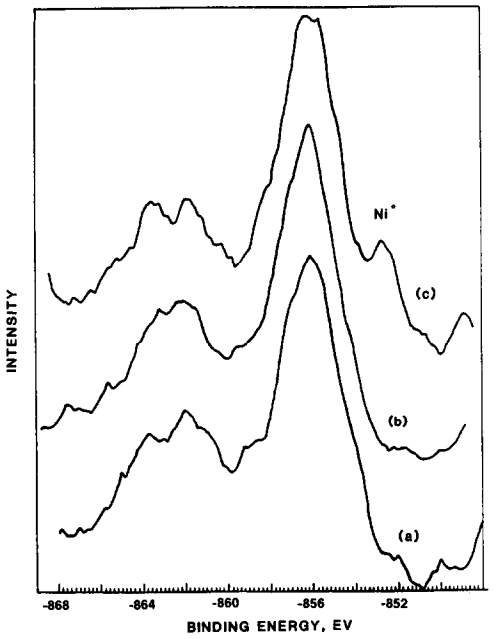

FIG. 3. Ni $2p_{3/2}$ spectra for the ground boron-containing catalysts (a) before and (c) after reduction. Reduction had no effects on the alumina-peptized catalyst (b).

Figure 5 shows the Mo 3*d* spectra. The boron-containing powder yields a Mo 3*d* spectrum less well defined than the one measured for the neat system; a slight shift to lower binding energy was also observed.

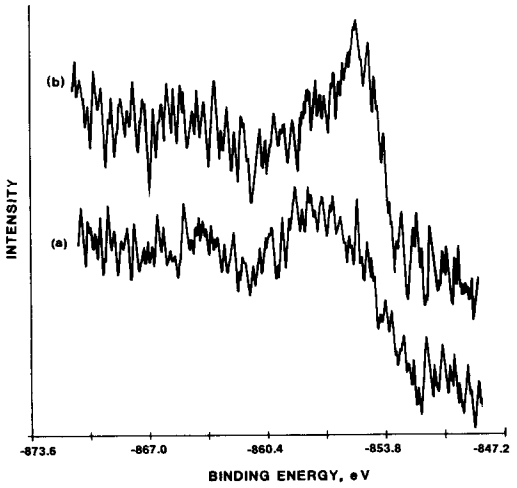

FIG. 4. Ni 2*p* spectra for the sulfided catalysts: (a) with boron and (b) without boron.

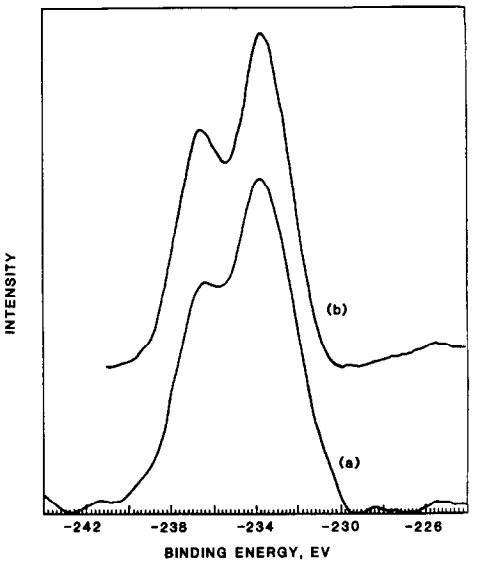

FIG. 5. Mo 3*d* spectra for two ground hydrotreating catalysts: (a) with boron and (b) without boron.

These results suggest that molybdenum is in more than one environment on the surface. A contribution from Mo(V) could explain the observed broadening and energy shift. Mo 3*d* spectra for the sulfided catalysts are shown in Fig. 6. The peak at 227 eV is assigned to the S 2*s* band. The peak at 228.5 eV is assigned to Mo $3d_{5/2}$ in MoS_2, that at 232.0 eV to unreacted Mo oxides. The peak at 236.0 eV suggests the presence of MoO_3. The B-containing catalyst has more Mo(VI) or Mo(V), while the Al-containing catalyst is richer in Mo(IV), suggesting the presence of weak Mo–support interactions which promote MoS_2 formation.

Table 5 summarizes the results of the XPS semiquantitative analysis. Precision of the method is ~5% while the accuracy of the method is ±10%. Aluminum, silicon, and oxygen concentrations are almost constant from sample to sample and from the exterior to the extrudate interior. The catalysts' high C levels result from the thermal decomposition under N_2 of the solvent (methanol) used during Ni loading. Their Si concentration is significantly lower than

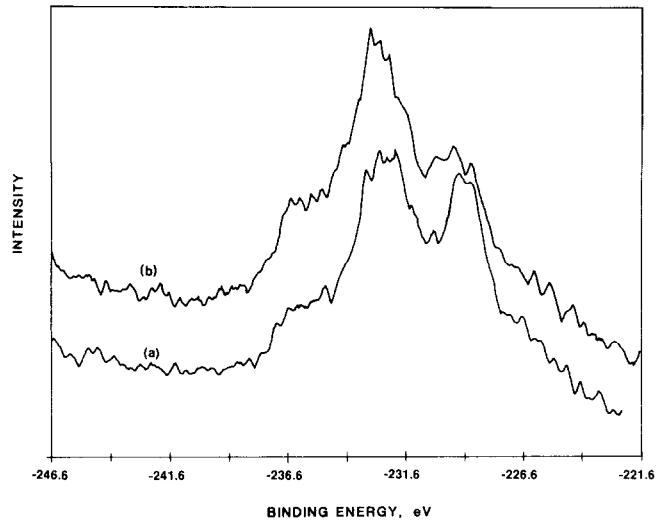

FIG. 6. Mo 3*d* spectra for the sulfided catalysts: (a) without boron and (b) with boron.

that expected (10–11 atom%) from bulk analysis data; the use of peptizing agents during the forming step could coat the zeolite surface with alumina and prevent Si detection.

Analyses for the ground and intact catalysts indicate that the extrudates surface is richer in boron than its interior. Boria melts at ~460°C and therefore could have migrated to the catalyst exterior during the 760°C calcination step. The lower metals concentration observed in the boron-containing catalyst surface (Table 5) is attributed to nickel and molybdenum migration in the macropores. As predicted by microprobe measurements (Fig. 2), the surface of the intact catalyst is richer in Mo than the surfaces of the ground material. The opposite is observed for Ni. This discrepancy could be due to Ni migration into the HY zeolite structure where it cannot be detected by XPS. The B-promoted surface is richer in Si than that of the B-free material, suggesting the presence of a greater zeolite concentration at the surface. Microprobe results in Fig. 1 and XPS data (Table 5) are in agreement for the $Al(NO_3)_3$-peptized catalyst.

TABLE 5

XPS Semiquantitative Analysis

Element	Concentration (at.%) ±10%			
	2% B		1% Al	
	Ground	Intact	Ground	Intact
Al	22.4	20.2	22.2	21.4
B	2.4	4.4	—	—
C	19.2	16.2	16.2	16.5
Mo	1.3	1.5	3.9	2.9
Ni	0.19	0.13	0.50	0.20
O	51.7	54.1	53.0	54.6
Si	2.8	3.5	3.5	2.9

Catalytic Activity

Under the mild hydrocracking conditions (1500 psig, 2000 scf H_2/bbl, LHSV = 2) used in catalyst screening and evaluation, it was found that boron addition has little effect on HDS, but it increases HDN activity. At 375°C, the nitrogen and sulfur content in an Agha Jari vacuum gas oil (Table 1), was reduced from 1500 and 17,500 ppm to 942 and 3800 ppm without boron and to 776 and 3700 ppm with boron. Similar results were obtained at higher (390°C) reactor temperature: nitrogen and sulfur levels dropped to

757 and 2000 ppm without boron and to 521 and 2100 ppm with boron.

The catalysts have similar cracking activity when used in upgrading a 260–426°C boiling range gas oil; chargestock inspections and testing methods are described elsewhere (*36*). Cracked products were found to contain nearly equal amounts of light cycle gas oil (LCGO is the 221–343°C cut), but exhibited different gasoline and slurry oil (SO is the 343–426°C cut) selectivities. The B-promoted catalyst cracks more SO and generates greater gasoline yields, suggesting that its macroporous structure sorbs and cracks high-molecular-weight hydrocarbons which the $Al(NO_3)_3$-peptized catalyst cannot.

Since the B-promoted catalyst's metals are segregated to the exterior, its hydrogenation centers will be more readily available than those of a catalyst in which metals are preferentially found in the interior. The existence of macropores which can sorb the larger N-containing molecules and greater metals availability is believed to enhance HDN activity. Hydrotreating conditions as well as feedstock compositon will control the magnitude of the effects that boron addition will have on catalyst performance.

CONCLUSIONS

Hydrotreating catalysts can be formed by incorporating zeolites (50 wt%) into an Al_2O_3 matrix by a forming method involving peptizing agents, mix-mulling, and a high-temperature calcination step prior to metals loading. Nickel is present as a pseudospinel identical to typical nickel on alumina systems. Molybdenum is present predominantly as the supported oxide. The better defined peak evident in Fig. 5 for the catalyst which does not contain boron suggests that molybdenum oxide island formation may be occurring. This is in contrast to the boron-containing catalyst which contains more than a single molybdenum environment. Several factors can affect the manner in which molybdenum is deposited. However, since the catalysts were prepared in exactly the same manner, it is believed that boric acid generates macropores and a surface acidity effect which can segregate metals (Ni and Mo) to the catalyst exterior. The macroporosity and greater metals availability is responsible for the enhanced HDN activity observed when upgrading a vacuum gas oil at mild hydrotreating conditions with the B-promoted catalyst.

ACKNOWLEDGMENTS

We would like to thank Dr. C. L. Kibby (GR&DC) and Dr. J. Stencel (DOE, Pittsburgh) for helpful discussions of XPS data. A special thanks is due to Professor D. Hercules (University of Pittsburgh) for critically reviewing this manuscript.

REFERENCES

1. Katzer, J. R., and Sivasubramanian, R., *Catal. Rev. Sci. Eng.* **20**(2), 155 (1979).
2. Houalla, M., *et al., Div. Pet. Chem. Prepr.* **22,** No. 3, 941 (1977).
3. Flinn, R. A., *et al., Hydrocarbon Process. Pet. Refin.* **42,** No. 9, 129 (1963).
4. Aboul-Gheit, A. K., *Canad. J. Chem.* **53,** 2575 (1975).
5. Stern, E. W., *J. Catal.* **57,** 390 (1979).
6. Satterfield, C. N., *et al., AIChE J.* **21,** No. 6, 1100 (1975).
7. Shih, S. S., *et al., Amer. Chem. Soc. Div. Pet. Chem. Prepr.* **22**(3), 914 (1977).
8. Sze, M. C., and Gelbein, A. D., U.S. Patent No. 4,108,761 (1978).
9. O'Hara, M. J., U.S. Patent No. 3,666,685 (1972).
10. Ward, J. W., U.S. Patent No. 4,120,825 (1978).
11. Bertolacini, R. J., U.S. Patent No. 4,211,634 (1980).
12. McArthur, D. P., U.S. Patent No. 4,034,061 (1977).
13. Pine, L. A., U.S. Patent No. 3,954,670 (1976).
14. Itoh, T., *et al.,* U.S. Patent No. 4,134,856 (1979).
15. Itoh, T., *et al.,* U.S. Patent No. 4,008,149 (1977).
16. O'Hara, M. J., U.S. Patent No. 3,666,685 (1972).
17. Tagari, O., *J. Jpn. Pet. Inst.* **22**(6), 336 (1979).
18. Ono, T., *et al., J. Jpn. Pet. Inst.* **23**(2), 110 (1980).
19. Nakamura, M., *et al., J. Jpn. Pet. Inst.* **26**(2), 108 (1981).
20. Togan, O., *et al., J. Jpn. Pet. Inst.* **26**(4), 226 (1981).
21. Pollard, R. J., and Veorhies, J. D., U.S. Patent No. 4,139,492 (1979).
22. Pine, L. A., U.S. Patent No. 3,993,557 (1976).
23. Pine, L. A., U.S. Patent No. 3,954,670 (1976).

24. Livingston, J. Y., *in* "Proceedings, 74th National AIChE meeting, New Orleans, Louisiana," March 11–15, 1973.
25. Van Zoonen, D., and Douwes, C. Th., *J. Inst. Pet.* **49,** 385 (1963).
26. Satchell, D., Ph.D. thesis. Oklahoma State University, 1974.
27. Kovach, S. M., *et al., Ind. Eng. Chem., Prod. Res. Dev.* **17,** 62 (1978).
28. Debies, T. P., and Schrall, D. M., *J. Electron Spectrosc.* **31,** 191 (1983).
29. Hair, M. L., and Hertl, W., *J. Phys. Chem.* **77,** 1965 (1973).
30. Cant, N. W., and Little, L. H., *Canad. J. Chem.* **43,** 1252 (1965).
31. Kieslev, A. V., *Discuss. Faraday Soc.* **52,** 14 (1971).
32. Wu, M., and Hercules, D. M., *J. Phys. Chem.* **83,** 2003 (1979).
33. Wu, M., *et al., Spectrosc. Lett.* **11,** 615 (1978).
34. Lojacono, M., *et al., J. Phys. Chem.* **75,** 1044 (1971).
35. Cimino, A., *et al., J. Phys. Chem.* **79,** 243 (1975).
36. Occelli, M. L., *I&EC Prod. Res. Dev. J.* **22,** 4 (1983).